Journal of Biomechanics 45 (2012) 895–902

Contents lists available at SciVerse ScienceDirect

Journal of Biomechanics

journal homepage: www.elsevier.com/locate/jbiomech
www.JBiomech.com

Quantification of embryonic atrioventricular valve biomechanics during morphogenesis

Philip R. Buskohl [a], Russell A. Gould [b], Jonathan T. Butcher [b,*]

[a] Department of Mechanical and Aerospace Engineering, Cornell University, Ithaca, NY 14853, USA
[b] Department of Biomedical Engineering, Cornell University, Ithaca, NY 14853, USA

ARTICLE INFO

Article history:
Accepted 1 July 2011

Keywords:
Pipette
Remodeling
Finite element
Simulation
Uniaxial
Endocardial cushions

ABSTRACT

Tissue assembly in the developing embryo is a rapid and complex process. While much research has focused on genetic regulatory machinery, understanding tissue level changes such as biomechanical remodeling remains a challenging experimental enigma. In the particular case of embryonic atrioventricular valves, micro-scale, amorphous cushions rapidly remodel into fibrous leaflets while simultaneously interacting with a demanding mechanical environment. In this study we employ two microscale mechanical measurement systems in conjunction with finite element analysis to quantify valve stiffening during valvulogenesis. The pipette aspiration technique is compared to a uniaxial load deformation, and the analytic expression for a uniaxially loaded bar is used to estimate the nonlinear material parameters of the experimental data. Effective modulus and strain energy density are analyzed as potential metrics for comparing mechanical stiffness. Avian atrioventricular valves from globular Hamburger–Hamilton stages HH25–HH34 were tested via the pipette method, while the planar HH36 leaflets were tested using the deformable post technique. Strain energy density between HH25 and HH34 septal leaflets increased 4.6 $\pm$ 1.8 fold ($\pm$ SD). The strain energy density of the HH36 septal leaflet was four orders of magnitude greater than the HH34 pipette result. Our results establish morphological thresholds for employing the micropipette aspiration and deformable post techniques for measuring uniaxial mechanical properties of embryonic tissues. Quantitative biomechanical analysis is an important and underserved complement to molecular and genetic experimentation of embryonic morphogenesis.

© 2011 Elsevier Ltd. All rights reserved.

1. Introduction

Morphogenetic events in the developing embryo are the result of dynamic interactions between cells and their environments. Many technologies exist to decipher the molecular and genetic regulation of cell behavior, but far less is known about the role of micro-environmental signaling. In the case of the heart, it is well known that virtually all mechanically relevant indices increase over development (e.g. blood pressure, wall shear stress, myocardial wall strain (Damon et al., 2009; Hu and Clark, 1989; Yalcin et al., 2011)). While it is appreciated that the resident tissue must somehow strengthen to withstand these increased loads, quantifying these material properties is extremely challenging. In the case of heart valve development, globular gelatinous masses, dubbed cushions, are rapidly remodeled into thin, fibrous leaflets, rich in matrix fiber striation (Camenisch et al., 2002; Person et al., 2005). In common animal models such as chick and mouse, these tissues barely reach beyond 1 mm in length, which is much too small for traditional uniaxial testing, but in general too large for AFM or optical trapping methods (Jastrzebska et al., 2006; Latinovic et al., 2010). Previous experiments have shown that many embryonic tissues including valves are super-compliant, with elastic moduli less than 40 Pa (Butcher et al., 2007; von Dassow et al., 2010). Unlike relatively stable postnatal tissues, the constant and significant shape and size change over time may selectively invalidate some testing methodologies.

Many techniques have been developed to assess the biomechanics of micro-scale tissues (generally a few millimeters or less in length). Pipette aspiration (PA) applies a local vacuum pressure and monitors resultant tissue displacement within the tip. PA has previously been used to measure material properties of early embryonic valve cushion primordia (Butcher et al., 2007), as well as adult pig and mice valves (Krishnamurthy et al., 2010; Zhao et al., 2011), and blood vessel walls (Ohashi et al., 2005). The ability to relate experimental data in these studies to meaningful material properties have varied. Early work derived Young's modulus, E, of a linear elastic material in terms of the applied

* Corresponding author at. 304 Weill Hall, 526 Campus Rd, Cornell University, Ithaca, NY 14853, USA. Tel.: +1 607 255 3575; fax: +1 607 255 7330.
E-mail address: jtb47@cornell.edu (J.T. Butcher).

0021-9290/$ - see front matter © 2011 Elsevier Ltd. All rights reserved.
doi:10.1016/j.jbiomech.2011.11.032

pressure, ΔP and aspirated length, L, for an infinite half-space undergoing small strain (Theret et al., 1988). While some recent studies utilize this model directly for tissues (Krishnamurthy et al., 2010), others have modified the approach to consider viscoelasticity (Merryman et al., 2009; Sato et al., 1990), different material layers (Alexopoulos et al., 2003), or pipette–tissue adhesion (Boudou et al., 2006). An early finite element (FE) analysis of the pipette method developed a similar small-strain expression for E for a finite tissue geometry (Aoki et al., 1997). Such soft tissues, however, predominantly demonstrate marked nonlinear material behavior with large deformations, and therefore need to be considered in a finite elasticity context. Recent inverse FE simulations enable nonlinear material property identification (Zhao et al., 2009; Zhao et al., 2011), but with significant time and computational resource cost. Though currently unknown, if the pipette technique could approximate a uniaxial tensile test at these length scales, a more straightforward and widely palatable experimental approach would be enabled.

A second common technique is the use of deformable microfabricated posts that measure applied force via traditional cantilever deflection. While commonly fabricated in a subcellular array to measure local cell traction forces (Legant et al., 2009; Tan et al., 2003), we hypothesized that a similar system could function for planar embryonic soft tissues like heart valve leaflets. Furthermore, by analyzing the two techniques (PA and deformable posts (PD)) with the same nonlinear material law, the acquired material parameters directly relate. This study pursues the above. We here establish the appropriate morphological regimes where each device is viable for stiffness measurement, and demonstrate their utility for soft, short length scale embryonic heart valve tissues. We further present strain energy as an alternative metric for representing stiffness for nonlinear materials.

2. Materials and Methods

2.1. Pipette aspiration (PA) experiments

2.1.1. PA simulation

A FE model of the pipette technique was developed to, (1) characterize the effects of tissue geometry on the experimental measurements of applied pressure and aspiration length, and (2) construct an analytical model to interpret the experimental data. In all simulations the tissue was modeled as an incompressible, isotropic, hyperelastic disk with thickness D, and radius R (see Fig. 1). A vacuum pressure, ΔP, was applied to the tissue surface in the pipette interior, and all exterior surfaces were assumed traction free. The pipette was modeled as an analytically rigid surface with filleted edges for smooth tissue contact. The pipette thickness was 25% of the pipette inner radius, r_p, comparable to the pipettes used in the experiments. Free-sliding contact was assumed between the tissue and pipette tip. An axisymmetric model using 2-D, 8 node quadrilateral, 2nd order elements with displacement–pressure (u–p) hybrid formulation were used for optimal handling of the incompressibility condition. FE simulations were performed in ANSYS v12.1 (ANSYS Inc., Canonsburg, PA) using approximately 3600 elements.

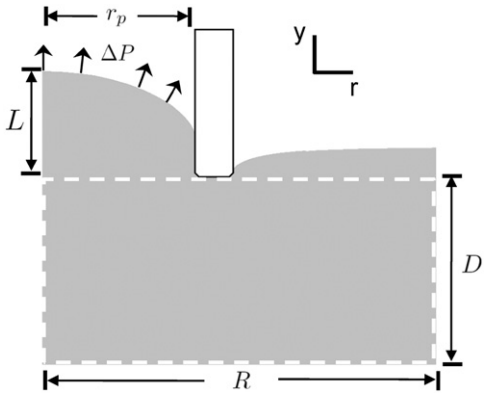

Fig. 1. Axisymmetric schematic of pipette aspirated tissue disk. The reference tissue is denoted by the dashed box and has dimensions of radius, R, and thickness, D. The region inside the pipette with radius, r_p, is loaded with aspiration pressure, ΔP, resulting in an aspirated length, L.

First, using a NeoHookean material law, the effect of tissue geometry was investigated by varying the ratio of tissue thickness and radius relative to the pipette radius, $\overline{D}=D/r_p$, and $\overline{R}=R/r_p$, respectively. The slopes of the ΔP versus λ curves, where $\lambda=(L+r_p)/r_p$ and L is the aspirated length, were evaluated to determine $\overline{D}$ and $\overline{R}$ regimes where PA yields consistent slope values. Second, to interpret the pipette data, FE results were compared to the analytical expression for the axial stress of a uniaxially loaded, incompressible bar (Eq. (2)). The NeoHookean ΔP versus λ curve was compared to the Cauchy and 1st Piola Kirchhoff (PK) stress measures. The ΔP versus λ curve was expected to best relate to the Cauchy stress, or "true stress", yet the projected area of loading is constrained by the pipette wall, motivating a comparison with the 1st PK, or "true force over original area". Third, given the exponential nature of the experimental data, an exponential material law (Zhao et al., 2011),

$$W=\frac{C}{2}\{\exp[\alpha(I_B-3)]-1\}, \tag{1}$$

was also analyzed via the USERHYPER subroutine, where $I_B=tr(\mathbf{F}\mathbf{F}^T)$, $\mathbf{F}$ is the deformation gradient, and α, C are material parameters. Agreement between the Cauchy stress, σ_{yy}, and the ΔP versus λ curve was also quantified for the exponential material law.

2.1.2. PA experiment technique

Avian left atrioventricular (AV) valve primordia mechanical properties were quantified using PA. Hamburger–Hamilton (HH) stages 25–34 septal and mural leaflets were isolated and placed directly in phosphate-buffered saline (PBS, Gibco) prior to testing. A glass micropipette ($r_p \geq 35$ μm) was placed adjacent to the cushion surface collinear with the AV canal axis for HH25, while it was placed on leaflet surface facing the atrium for HH29 and HH34. Vacuum pressure was incrementally applied via a 200 μL pipetter calibrated with a custom manometer. Previous strain history was mitigated by preconditioning with ~20 cycles of low pressurization (< 1 Pa). The preconditioning step ensured the tissue and pipette tip were in full contact. Incremental pressure loads were then applied, at which images were captured for each static load at 150 × magnification using a Zeiss Discovery v20 stereo microscope (Spectra Services, Inc.). The aspirated length was measured using calibrated images in NIH ImageJ.

An experimental "stretch ratio", $\lambda=(L+r_p)/r_p$ was defined by normalizing the aspirated length to the pipette radius. The experiment stretch ratio is a measure of geometry change during aspiration, which is related, but not identical to the local stretch of the tissue (see Supplemental Fig. S3B). The ΔP versus λ curves were fit using the axial Cauchy stress for a uniaxial load of an incompressible material with an assumed exponential material law (Eq. (1)), specifically,

$$\sigma_{yy}=\alpha C\exp\left[\alpha\left(\lambda^2+\frac{2}{\lambda}-3\right)\right]\left(\lambda^2-\frac{1}{\lambda}\right) \tag{2}$$

The fitting parameters α and C were determined by minimizing the sum of the errors squared between Eq. (2) and the ΔP versus λ data curves. The C parameter was modified using a scale factor determined from FE simulation, $C_{mod}=\gamma(\alpha)C$. Effective modulus, $E_{Eff}=\alpha C_{mod}$, and strain energy density were evaluated as metrics for comparing mechanical testing data. Strain energy density (Pa or kPa) was calculated as the stored energy of the uniaxial deformation with axial stretch ratio ranging from $\lambda=[1,2]$, namely $W_{1-2}=(C_{mod}/2)\{\exp(2\alpha)-1\}$. Data is presented with representative stress response curves and strain energy density values presented as mean ± SD with $n=8$–11. Statistical comparisons were performed using ANOVA with Tukey post-tests or Student's t-test, $^*p<0.05$.

2.2. Deformable post (DP) experiments

To measure mechanical properties of planar tissue, a custom device was fabricated which measured force based on beam deflection theory. Deformable cantilevers constructed from polydimethylsiloxane (PDMS, Sylgard 184) were used to determine the forces in the micro–milliNewton range (μ–mN). To create the DPs, negative molds were machined into a Teflon block. For this study, we generated three different size posts, all with a height, h_p, to diameter, ϕ_p, ratio of three (3 mm/1 mm, 6 mm/2 mm, 9 mm/3 mm). However, the 3 mm/1 mm cantilever was optimal, due to the size and generated force range of the HH36 valves. The PDMS was mixed at a ratio of 10:1 (base/curing agent), poured into mold geometry, cured at 65 °C for 12 h, and then autoclaved to complete curing process. Post bending stiffness and batch variability were measured using a previously described method (Sasoglu et al., 2007). Filter paper patches (CFP4, Whatman) were secured to the top of each post to provide a substrate for tissue attachment. The silicone posts were mounted on two horizontal sliding arms, which were capable of positive and negative translation. The freshly isolated HH36 valves were delicately transferred to a glass slide using a transfer pipette, and the residual saline was wicked away. The glass slide was then inverted, placed over

the DP, and leaflet edges brought in contact with filter paper. Once the valve was placed across the DPs in a planar fashion, two small drops of cyanoacrylate (454 Prism, Loctite), applied with micropipette (100 μm diameter), secured the valve to the DP. The mechanical testing was then conducted in PBS at 20 °C. Deflection was determined as half the difference between the displacements of the base and the tip of the post, specifically, $v=(x_b-x_t)/2$ (Fig. 6A). From the deflection and the bending stiffness calibration, the axial force in the plane of the tissue was approximated. The axial force was normalized to initial reference area, approximated as the product of the unloaded thickness and width. An average stretch ratio for the deformable post tissue was defined as $\lambda_p=(x_t-x_0)/x_0$. The 1st PK form of the axial stress for a uniaxial load, (Eq. 2), was used to fit the post data. The 1st PK stress versus λ_p curves are presented for the HH36 septal leaflet along with the average W_{1-2} value for $n=9$.

2.2.1. DP simulation

A FE model of a post with fixed base and transverse applied force at tip was investigated. The post was modeled as an incompressible, NeoHookean material using 8 node 3D solid structure elements with u–p formulation. Force–deflection profiles were calculated for differing post geometries by varying post height and diameter. Scaling of bending stiffness between differing post geometries was compared to Euler beam theory. The analysis was performed to determine maximum tissue contact area within the required force transduction range. Maximal contact area is beneficial for the attachment of tissue to the DPs.

2.3. AV cushion geometry transition

The geometries of AV valve primordia were measured for HH25, HH29, HH34, and HH36 embryonic stages. Cushion length, L_c, was taken to be the dimension protruding perpendicular from the AV canal wall. Thickness, t_c, was the cushion dimension perpendicular to L_c along the anterior–posterior axis. Lastly cushion width, w_c, was defined as the maximum dimension of the cushion along the dorsal–ventral axis of the heart. Measurements were taken from magnified images of cushions immediately after isolation using Zeiss Discovery v20 stereo microscope and ImageJ.

3. Results

3.1. Pipette stiffness results are sensitive to tissue geometry

The geometry of aspirated tissues, both thickness and radius, can influence pipette stiffness measurements. FE simulations with a NeoHookean material demonstrate that the slope of ΔP versus λ decreases as tissue thickness, $\overline{D}=D/r_p$, goes to zero (Fig. 2A). The measured stiffness decreases rapidly for $\overline{D}<2$, with a 50% decrease between $\overline{D}=2$ and $\overline{D}=0.75$. The decrease in stiffness is a direct result of higher aspirated lengths, due to contributions from tissue bending. Evidence for bending is seen in the change of sign ($\pm$) of the radial stress ($\hat{\sigma}_{rr}$) along the axis of symmetry for tissue thickness $\overline{D}\leq 2$ (Fig. 2B). The pipette aspiration method assumes local stretching at the location of applied pressure, not bending of the global tissue. While the error in stiffness measurement between $\overline{D}=2$ and $\overline{D}=4$ may be small (~2%), the assumption of no tissue bending is not valid until $\overline{D}\geq 4$. Similarly, measured stiffness decreases as tissue radius $\overline{R}=R/r_p$ approaches unity (Supplemental Fig. S1). Measured stiffness values converged for $\overline{R}\geq 2$, but errors were introduced for smaller $\overline{R}$. The maximum error calculated was 9.7% between $\overline{R}=1.25$ and $\overline{R}=2$.

3.2. PA approximates uniaxial deformation in tissue interior

FE simulations of the pipette method, using either NeoHookean or exponential material laws (Eq. (1)), demonstrate a heterogeneous strain field, with maximum magnitudes located at the contact surface between the tissue and the pipette (Supplemental Fig. S2). Near the axis of symmetry the strain field is more uniform, with the only significant gradient in the y direction. The radial and meridian stretch ratios, λ_r and λ_θ, respectively, along the axis of symmetry were equal and transitioned from elongation to compression with depth into tissue (Fig. 3A). Conversely, the stretch in the y direction, λ_y, was in compression at the pressurized tissue surface, but transitioned toward elongation in the tissue interior. This depicts a transition from equibiaxial extension (gray region Fig. 3A) toward uniaxial with depth. The y location of this transition y_{trans} varies with applied load, but remains near the surface, never exceeding $r_p/2$ in any of the simulations and therefore lying within the initial "cap" of distended tissue (Supplemental Fig. S3A). The geometric "stretch ratio" $\lambda=(L+r_p)/r_p$ was implemented to approximate the y-axis stretch, which varied with depth along the axis of symmetry. The average of λ_y along the axis of symmetry was always greater than or equal to one, and was linearly related to λ (Supplemental Fig. S3B).

3.3. ΔP proportional to axial stress of uniaxial deformation

An analytic model was developed, for the purpose of interpreting the experimental data, by comparing the pipette pressure ΔP versus λ to the axial stress versus axial stretch of a uniaxial load (Eq. (2)). FE generated ΔP versus λ curves aligned closest to the axial Cauchy stress, σ_{yy} for the NeoHookean material, not with the 1st PK (Fig. 3B). The slopes of the ΔP versus λ and the σ_{yy} versus λ curves differed by a factor, which correlated with the stiffness offset from unity for $\overline{D}>4$ seen in Fig. 2A. Similarly, with the exponential material, the ΔP versus λ curve differed only by a scalar factor from

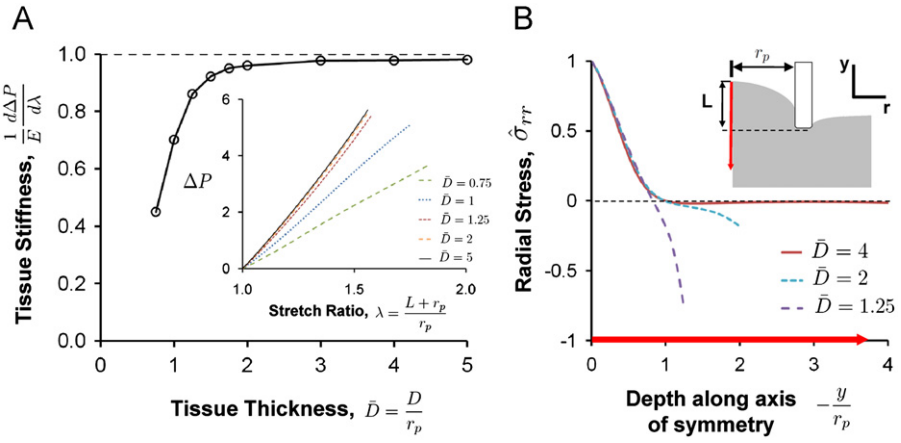

Fig. 2. Pipette stiffness measurements consistent for $D>4\ r_p$. (A) Plot of measured tissue stiffness normalized to Young's Modulus, E, of a NeoHookean material versus tissue thickness, $\overline{D}$. Inset: FE generated ΔP versus λ curves from which stiffness was calculated from the slope. (B) Plot of radial stress normalized to stress at applied load surface as a function of depth along the axis of the symmetry. For $\overline{D}<4$, the radial component (likewise meridianal) experiences a compressive stress at the bottom edge, evidence of the tissue undergoing bending.

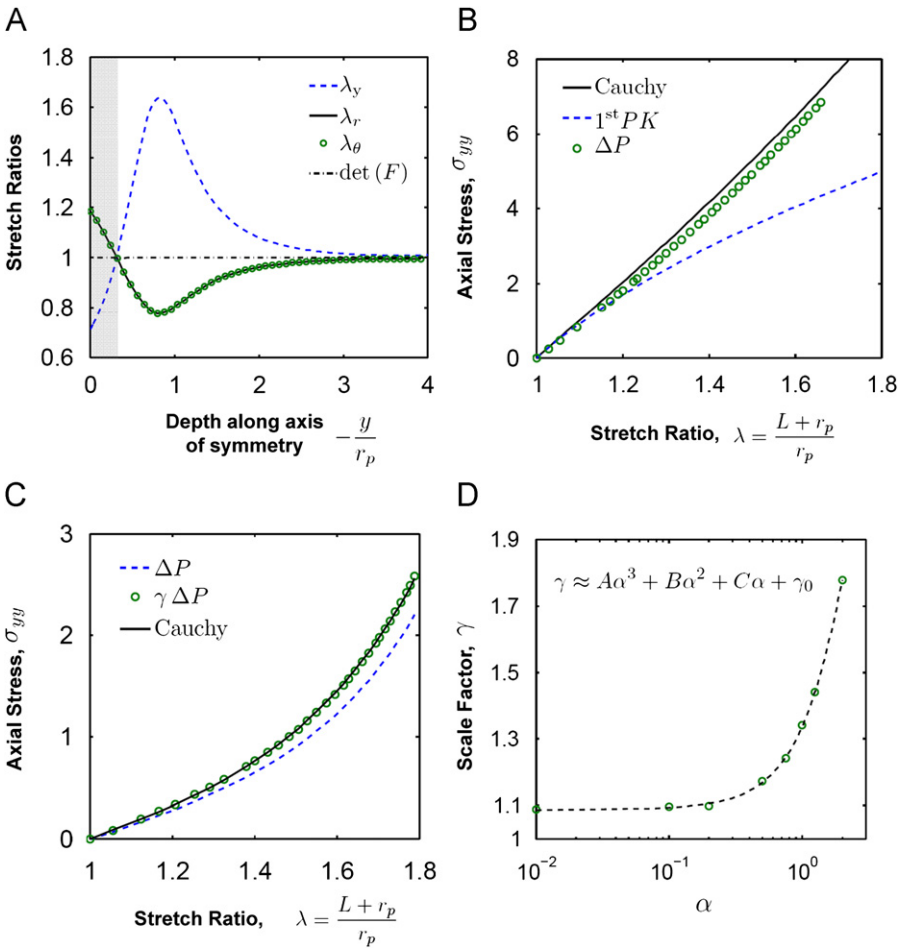

Fig. 3. Pipette aspiration approximated as a uniaxial load. (A) Along the axis of symmetry, the deformation transitions from equibiaxial (gray region) extension toward uniaxial extension with depth into the tissue. (B) The ΔP versus λ curve of an incompressible, NeoHookean material closely aligns with the Cauchy stress of a uniaxially loaded bar, not the 1st Piola-Kirchhoff stress. (C) The ΔP versus λ curve of an exponential material differs by a scale factor, γ, from the axial stress of a uniaxial load compared at same stretch ratio. (D) The scale factor, γ, is a function of only α, which is approximated with the cubic polynomial shown for α in [0, 2]. $A=-0.052$, $B=0.252$, $C=0.053$, and $\gamma_0=1.09$.

the assumed uniaxial model (Fig. 3C). A parameter sweep of both α and C demonstrated that the scale factor γ for the exponential material was only a function of α (parameter range $C \in [0.01–100]$ and $\alpha \in [0.01–5]$). The relationship between α and the scale factor was fit to cubic order polynomial: $\gamma = A\alpha^3 + B\alpha^2 + C\alpha + \gamma_0$, where $A=-0.052$, $B=0.252$, $C=0.053$, and $\gamma_0=1.09$ (Fig. 3D). For $\alpha > 2$, the fit quality between the simulation and analytic model was unsatisfactory, hence $\alpha=2$ was considered an upper bound for relating PA to a uniaxial load test.

3.4. Strain energy density as an alternative stiffness metric

An effective modulus, $E_{Eff}=\alpha C$, has been suggested as a stiffness metric for two parameter exponential models (Butcher et al., 2007; Zhao et al., 2011). For small α, ($\alpha < \sim 0.2$), E_{Eff} approximates the slope of ΔP versus λ, as the curve is nearly linear. Unfortunately, $\alpha < 0.2$ is too strict a condition for sufficient curve fitting of experimental data, and E_{Eff} loses its physical significance outside this range. Furthermore, E_{Eff} is not a unique parameter, as an infinite combination of α and C values will equal the same E_{Eff} value. Strain energy density is therefore proposed as an alternative, physically significant, metric for comparing mechanical properties. Continuing with the uniaxial analog, the strain energy density from $\lambda=[1,2]$ has a simple form: $W_{1-2} = (C_{mod}/2)\{\exp(2\alpha)-1\}$. This strain energy parameter is also not unique, but over a given set of α values it produces a narrower range of material response curves than the corresponding curves for fixed E_{Eff} (Fig. 4). For $\alpha=0.5,1,1.5$, and 2, the range of material response curves with fixed $E_{Eff}=1$ is quite wide with approximately a 3 fold difference in strain energy density,

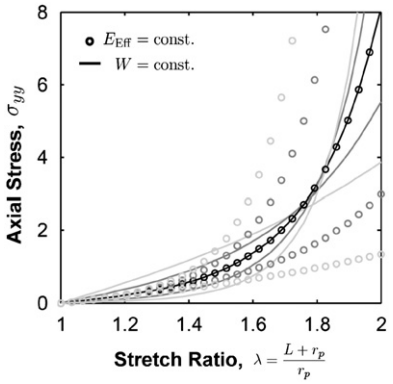

Fig. 4. Strain energy density is a meaningful parameter for nonlinear material comparison. Plot of axial Cauchy stress for an exponential material with (1) fixed effective modulus, $E_{Eff}=\alpha C$ (circles), and (2) fixed strain energy density from λ_{1-2} (solid lines) evaluated for $\alpha=0.5$, 1, 1.5, and 2. Though both parameters are non-unique, the strain energy density generates a tighter range of material response curves over the same set of α values, while E_{Eff} has a larger spread of material response curves and no physical meaning for large α.

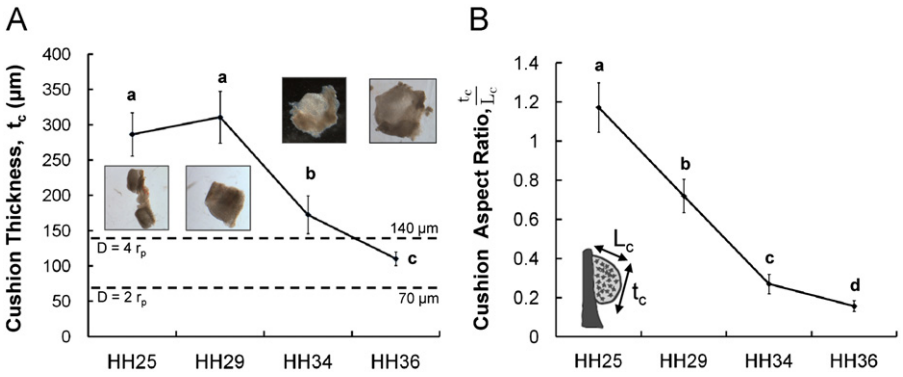

Fig. 5. AV cushion geometry transition necessitates alternative mechanical testing devices. (A) Cushion thickness, t_c, relative to pipette placement decreases during development. HH36 violates the $D=4r_p$ testing criteria for 70 μm pipette diameter. (B) Ratio of cushion thickness over cushion apex to base length, L_c, shows a transition to a more planar configuration at the completion of valvulogenesis (HH36). $n=8$–10 mean ± SD, all pairs of different letters are statistically significant, ANOVA, $p<0.001$.

while for fixed W_{1-2} the curve spread is tighter. The enhanced consistency of strain energy density at these higher α values gives it an advantage over E_{Eff}, even if not a direct measure of stiffness.

3.5. Globular to planar geometry transition is concomitant with stiffness increase

AV leaflet thickness decreased 3-fold from stage HH25 to HH36 (Fig. 5A), ending with a thickness of 110.4 ± 9.7 μm (mean ± SD) at HH36. With the $\overline{D}\geq 4$ criteria and assuming continuum measurements require $r_p\geq 35$ μm, the pipette method is best suited for leaflet thickness greater than 140 μm. Hence HH36 tissue was tested using the deformable post test device. The significant decrease in leaflet thickness was concomitant with 2.46 ± 0.28 and 1.85 ± 0.18 (fold ± SD) increases in leaflet length, L_c and width, w_c, respectively. The thickness to length ratio, t_c/L_c, decreased 6 fold from HH25 to HH36 as the globular cushion transitions into a planar leaflet (Fig. 5B). This shift of aspect ratio occurs over five days of development, underscoring the rapidity of this complex morphogenesis. The ΔP versus λ curves from the pipette data demonstrate a nonlinear, exponential behavior (Fig. 7A), with increased slope with development stage. The strain energy density increased 4.6 ± 1.8 fold (± SD) between HH25 inferior and HH34 septal cushions (Fig. 7B). Similarly, the HH29 septal cushion increased 2.5 ± 0.9 fold from the HH25 inferior cushions. The HH25 superior cushion was slightly stiffer than the inferior cushion with strain energy density of 0.44 ± 0.14 Pa versus 0.34 ± 0.08 Pa (mean ± SD). Mural leaflet strain energy increased from 0.69 ± 0.11 Pa to 0.96 ± 0.21 Pa between HH29 and HH34. The mural and septal leaflet strain energies only differed statistically at HH34. The HH36 septal material behavior well fit the 1st PK stress for a uniaxial load of the exponential material law used to model the pipette experiment (Fig. 7C). The average strain energy density of the HH36 cushion in the plane of the tissue was $W_{1-2}=59.2\pm 14.2$ kPa. The in-plane strain energy density at HH36 was 4 orders of magnitude greater than the strain energy density in the transverse direction measured by PA.

3.6. DP force range is tunable according the Euler beam theory

The HH36 AV leaflets were tested with a DP uniaxial testing device (Fig. 6B and C). FE simulations demonstrated that for ratios of post height to diameter, $(h_p/\varnothing_p)>2$, the force versus deflection curve agreed with the Euler bending theory up to a deflection of $v=h_p/4$. For constant $h_p/\varnothing_p$, the bending stiffness scales linearly with cantilever diameter (Fig. 6D). For diameters 1, 2, and 3 mm, the bending stiffness was measured as 10.3 ± 1.5, 20.2 ± 1.9, and 29.9 ± 0.9 mN/mm, respectively (mean ± SD $n=6$). The small deviations in bending stiffness demonstrate the consistency of the fabrication technique and the low variability between silicone batches.

4. Discussion

Increasing evidence in developmental biology suggests that mechanical cues from the microenvironment are instrumental in directing cardiogenesis (Hove et al., 2003; Sedmera et al., 1999). Furthermore, the pivotal role AV valves play in manipulating blood flow highlights the importance of understanding their mechanical behavior even in the embryonic period (Vermot et al., 2009). The results of this study demonstrate that PA and DP techniques are effective and complimentary for quantifying the ultra-compliant properties of complex shaped, microscale, and embryonic tissues.

We confirmed the previously shown result that tissue thickness less than two pipette radii influences measured aspiration length (Aoki et al., 1997; Zhao et al., 2011). However, as shown in Fig. 2B, compressive stress occurs in the radial direction when $\overline{D}<4$. This compressive stress denotes global bending which elevates the measured aspiration length because tissue is deflecting, as well as stretching into the pipette. Therefore a $\overline{D}\geq 4$ criterion ensures no error due to tissue thickness. This criterion was satisfied for HH25–HH34 AV cushion, but the more planar HH36 tissue required a different technique. Furthermore, we show that the radial dimension of the tested tissue must exceed $R=2r_p$ for consistent results, though the errors introduced are not as large as those for the thickness criteria. This supports and extends recent work by Zhao et al. (2011) who considered material nonlinearity through the implementation of an exponential hyperelastic material law in an inverse FE analysis. In the current approach, we related the ΔP versus λ data from the pipette experiment to the Cauchy stress curve of a uniaxial load through a numerically determined scale factor. This result simplified the determination of α, C to an error minimization of an analytic expression, potentially saving significant post-testing computation time of inverse approaches. This also opens the PA approach to more developmental biology labs with likely limited computational expertise. It is important to note that our uniaxial approximation was valid for $\alpha<2$. While satisfactorily fitting the AV cushion data, utilization of a FE inverse approach would be necessary for tissues with larger α.

PA has previously been compared to equibiaxial loading (Evans and Waugh, 1977), which was in the context of red cell mechanics, where in-plane membrane surface tensions were assumed to dominate. For solid tissues with finite thickness,

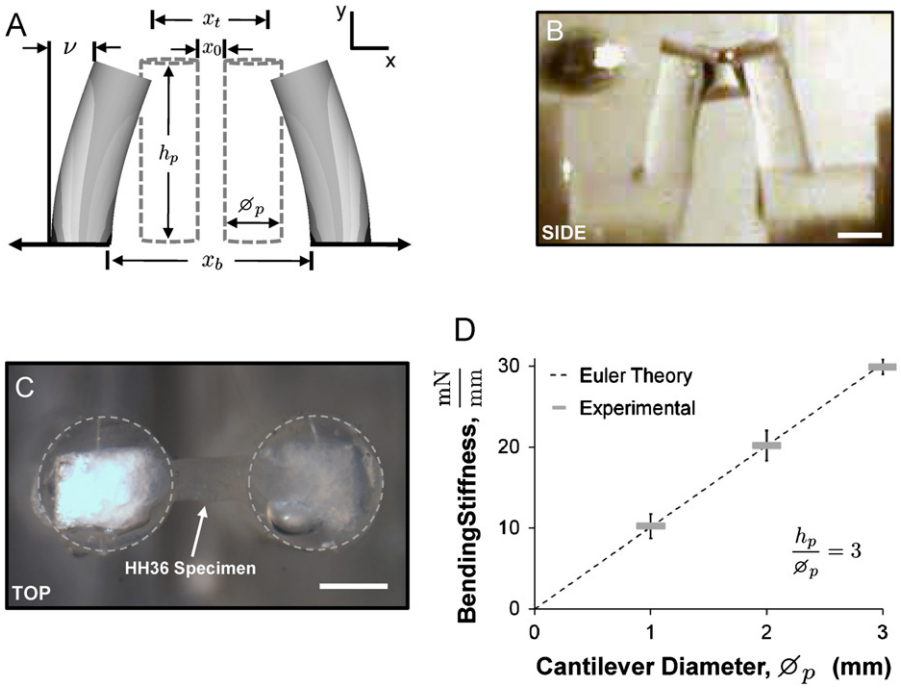

Fig. 6. Deformable post testing device for planar tissues. (A) Schematic of deformable cantilevers of height, h_p, and diameter, $\varnothing_p$, in reference (dashed) and deformed configurations (solid). DP deflection equals $\nu=(x_b-x_t)/2$, where x_t is the distance between the top of the posts, and x_b is the distance between the bases. (B) Side view of DP device, scale bar=1 mm (C) Top view of device with attached HH36 septal leaflet, and tip of posts highlighted for reference (dashed circles). Scale bar=500 μm. (D) Euler beam theory (dashed line) predicts a linear increase in bending stiffness with diameter for a fixed $h_p/\varnothing_p$. Measured bending stiffness for three diameters with $h_p/\varnothing_p=3$ showed agreement with theory, $n=6$ (3 silicone batches) mean ± SD.

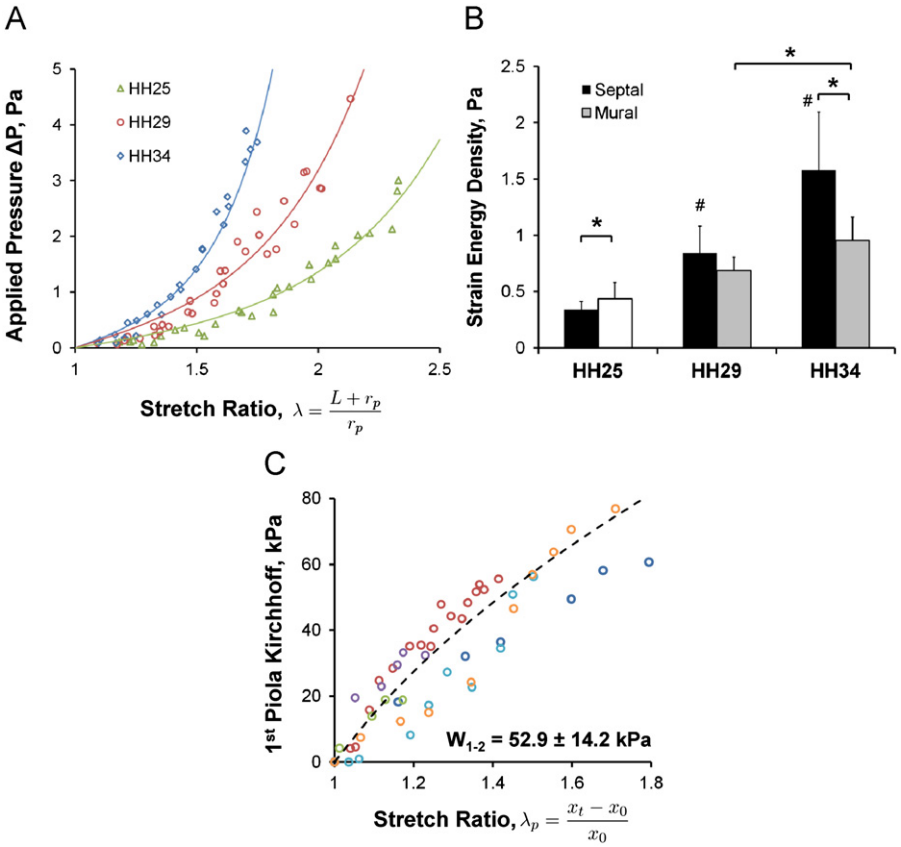

Fig. 7. Monotonic increase in AV cushion stiffness during development. (A) Representative PA data for septal leaflets from stages HH25–HH34, ($n=4$) (B) Calculated strain energy densities for septal (black) and mural (gray) cushions. HH25 inferior denoted as septal (black) and superior (white) bar. $n=8$–11 mean ± SD 1-way ANOVA or t-test $^*p<0.05$, # $p<0.001$ w.r.t. HH25 septal (C) Plot of applied force over initial cross-sectional area (~1st PK) for HH36 septal leaflet deformable post data. Average strain energy density denoted on figure as mean ± SD.

deformation along the pipette axis must be considered. Our FE simulations determined that the mode of deformation quickly transitioned from equibiaxial at the pressurized surface "cap" to uniaxial within the tissue along the axis of symmetry (Fig. 3A). The equibiaxial regime was very narrow ($y_{trans} < r_p/2$), and did not experience the high stretch ratios seen in λ_y in the tissue interior. This supports and extends the previous findings by Aoki et al., who suggested that the normal extension and shear components in the axial direction were the dominant contributions to the strain energy (Aoki et al., 1997). Taken together, these results support the uniaxial model as an intuitive and computationally inexpensive way to identify the material parameters of nonlinear materials.

Nonlinear material models lack direct, simple stiffness metrics for comparing test samples. Exponential, or Fung-like, materials are particularly difficult, as even linear fitting of sections of the stress–strain curve require tedious (and arbitrary) conditions to consistently apply fits (i.e. where does the toe region end, does a bi-linear fit effectively capture material nonlinearity, etc.). Others have compared stress values at a particular stretch (Liu and Fung, 1993), but this does not communicate the stress response curve nonlinearity. An effective modulus, E_{Eff}, defined as the product of the fit parameters, has previously been used as a stiffness measure for an exponential material model (Butcher et al., 2007; Zhao et al., 2011). Yet E_{Eff} only relates directly to stiffness for small α and is non-unique, prompting instead our analysis of strain energy density to compare samples. Our results determined that strain energy density was a much more consistent metric of tissue stiffness for a given material response (Fig. 4). This parameter is similar to toughness measures used in fracture mechanics, except here it is integrated only to a non-failure strain to approximate material behavior in physiological conditions.

Experiments using the PA method showed a stiffness increase over embryonic AV cushion valvulogenesis. The over 4-fold stiffness increase between HH25 and HH34 septal cushions is indicative of substantial biomechanical remodeling of the microstructure. Similar rates of stiffness increases in earlier embryonic stage AV cushions have been reported (Butcher et al., 2007). AV valves of fetal chick and mice have demonstrated an increase in extracellular matrix (ECM) protein synthesis, particularly in the collagen and elastin structural protein families (Kruithof et al., 2007; Peacock et al., 2008), as well as their structural organization (Hinton et al., 2006; Hurle et al., 1980). The mural leaflet stiffness lags the septal leaflet stiffness at HH34, potentially a result of differing progenitor origins (de Lange et al., 2004). The in-plane stiffness of the HH36 valves was approximately four orders of magnitude larger than all the pipette data sets. This indicates that tissue anisotropy is significant by HH36, with in-plane stiffness the dominant player. FE simulations of a linear elastic, transversely isotropic material showed that the transverse stiffness contributed one fifth of the measured stiffness compared to four fifths from the stiffness in the direction of the pipette axis (Ohashi et al., 2005). The effect of a nonlinear, highly aniosotropic tissue on measured stiffness with the pipette method is unclear, but could potentially be teased out with a more complicated FE simulation.

As the valve transitions toward a planar geometry, the tissue thickness criteria and continuum testing assumption become mutually exclusive. The DP device effectively measured tissue stiffness in this planar regime. Tan et al. first used this approach at the cellular scale, to measure sub-cellular traction forces (Tan et al., 2003). By constructing an array of micro-fabricated DPs (length 11 μm), mechanical interactions between cells and their underlying substrates were possible to measure through the DP deflection. Furthermore, DP bending rigidity could be easily tuned by altering their geometry (Fu et al., 2010). DPs have also been used to test the mechanical properties of microscale constructs of cells embedded within 3D matrices (Legant et al., 2009; Legant et al., 2010). During the remodeling of 3D collagen matrices, cellular contractile forces and changes in tissue morphology was quantified through the deflection of DPs of length 250 μm. By securing the HH36 embryonic tissue between DPs of length 3 mm, deflection of the silicone cantilevers provided a precise measurement of force within the mN range. Although this system was used for embryonic valves, it could be easily applied to other embryonic tissues.

In conclusion, PA and the DP techniques are two viable methods for evaluating the mechanical properties of ultra-soft, small-sized globular and planar tissues, respectively. AV cushions rapidly increase in stiffness during valvulogenesis, keeping pace with the demanding mechanical loading of its microenvironment. Selection of pipette dimension and point of application on tissue surface require consideration of an appropriate continuum approximation and specimen geometry, especially thickness. Strain energy density is a physically meaningful parameter for which to compare tissue stiffness, and can translate to any material model. Both techniques are applicable to soft, short length scale tissues, and further integration of the devices data sets will provide a richer understanding of other tissues with complex material properties.

Conflict of interest statement

There are no conflicts of interest to report.

Acknowledgments

We acknowledge support from the American Heart Association (AHA) SDG #0830384N, the National Science Foundation (NSF) GK-12 Fellowship #DGE 0841291 and NSF CAREER Award, and the National Institutes of Health (HL110328).

Appendix A. Supplementary information

Supplementary data associated with this article can be found in the online version at doi:10.1016/j.jbiomech.2011.11.032.

References

Alexopoulos, L.G., Haider, M.A., Vail, T.P., Guilak, F., 2003. Alterations in the mechanical properties of the human chondrocyte pericellular matrix with osteoarthritis. Journal of Biomechanical Engineering 125, 323–333.

Aoki, T., Ohashi, T., Matsumoto, T., Sato, M., 1997. The pipette aspiration applied to the local stiffness measurement of soft tissues. Annals of Biomedical Engineering 25, 581–587.

Boudou, T., Ohayon, J., Arntz, Y., Finet, G., Picart, C., Tracqui, P., 2006. An extended modeling of the micropipette aspiration experiment for the characterization of the Young's modulus and Poisson's ratio of adherent thin biological samples: numerical and experimental studies. Journal of Biomechanics 39, 1677–1685.

Butcher, J.T., McQuinn, T.C., Sedmera, D., Turner, D., Markwald, R.R., 2007. Transitions in early embryonic atrioventricular valvular function correspond with changes in cushion biomechanics that are predictable by tissue composition. Circulation Research 100, 1503–1511.

Camenisch, T.D., Molin, D.G., Person, A., Runyan, R.B., Gittenberger-de Groot, A.C., McDonald, J.A., Klewer, S.E., 2002. Temporal and distinct TGFbeta ligand requirements during mouse and avian endocardial cushion morphogenesis. Developmental Biology 248, 170–181.

Damon, B.J., Remond, M.C., Bigelow, M.R., Trusk, T.C., Xie, W., Perucchio, R., Sedmera, D., Denslow, S., Thompson, R.P., 2009. Patterns of muscular strain in the embryonic heart wall. Developmental Dynamics: An Official Publication of the American Association of Anatomists 238, 1535–1546.

de Lange, F.J., Moorman, A.F., Anderson, R.H., Manner, J., Soufan, A.T., de Gier-de Vries, C., Schneider, M.D., Webb, S., van den Hoff, M.J., Christoffels, V.M., 2004.

Lineage and morphogenetic analysis of the cardiac valves. Circulation Research 95, 645–654.
Evans, E.A., Waugh, R., 1977. Osmotic correction to elastic area compressibility measurements on red cell membrane. Biophysical Journal 20, 307–313.
Sasoglu, F.M., et al., 2007. Design and microfabrication of a high-aspect-ratio PDMS microbeam array for parallel nanonewton force measurement and protein printing. Journal of Micromechanics and Microengineering 17, 623.
Fu, J., Wang, Y.K., Yang, M.T., Desai, R.A., Yu, X., Liu, Z., Chen, C.S., 2010. Mechanical regulation of cell function with geometrically modulated elastomeric substrates. Nature Methods 7, 733–736.
Hinton Jr, R.B., Lincoln, J., Deutsch, G.H., Osinska, H., Manning, P.B., Benson, D.W., Yutzey, K.E., 2006. Extracellular matrix remodeling and organization in developing and diseased aortic valves. Circulation Research 98, 1431–1438.
Hove, J.R., Koster, R.W., Forouhar, A.S., Acevedo-Bolton, G., Fraser, S.E., Gharib, M., 2003. Intracardiac fluid forces are an essential epigenetic factor for embryonic cardiogenesis. Nature 421, 172–177.
Hu, N., Clark, E.B., 1989. Hemodynamics of the stage 12 to stage 29 chick embryo. Circulation Research 65, 1665–1670.
Hurle, J.M., Icardo, J.M., Ojeda, J.L., 1980. Compositional and structural heterogenicity of the cardiac jelly of the chick embryo tubular heart: a TEM, SEM and histochemical study. Journal of Embryology and Experimental Morphology 56, 211–223.
Jastrzebska, M., Zalewska-Rejdak, J., Mroz, I., Barwinski, B., Wrzalik, R., Kocot, A., Nozynski, J., 2006. Atomic force microscopy and FT-IR spectroscopy investigations of human heart valves. General Physiology and Biophysics 25, 231–244.
Krishnamurthy, V.K., Guilak, F., Narmoneva, D.A., Hinton, R.B., 2010. Regional structure-function relationships in mouse aortic valve tissue. Journal of Biomechanics.
Kruithof, B.P., Krawitz, S.A., Gaussin, V., 2007. Atrioventricular valve development during late embryonic and postnatal stages involves condensation and extracellular matrix remodeling. Developmental Biology 302, 208–217.
Latinovic, O., Hough, L.A., Daniel Ou-Yang, H., 2010. Structural and micromechanical characterization of type I collagen gels. Journal of Biomechanics 43, 500–505.
Legant, W.R., Miller, J.S., Blakely, B.L., Cohen, D.M., Genin, G.M., Chen, C.S., 2010. Measurement of mechanical tractions exerted by cells in three-dimensional matrices. Nature Methods 7, 969–971.
Legant, W.R., Pathak, A., Yang, M.T., Deshpande, V.S., McMeeking, R.M., Chen, C.S., 2009. Microfabricated tissue gauges to measure and manipulate forces from 3D microtissues. Proceedings of the National Academy of Sciences of the United States of America 106, 10097–10102.
Liu, S.Q., Fung, Y.C., 1993. Material coefficients of the strain energy function of pulmonary arteries in normal and cigarette smoke-exposed rats. Journal of Biomechanics 26, 1261–1269.
Merryman, W.D., Bieniek, P.D., Guilak, F., Sacks, M.S., 2009. Viscoelastic properties of the aortic valve interstitial cell. Journal of Biomechanical Engineering 131, 041005.
Ohashi, T., Abe, H., Matsumoto, T., Sato, M., 2005. Pipette aspiration technique for the measurement of nonlinear and anisotropic mechanical properties of blood vessel walls under biaxial stretch. Journal of Biomechanics 38, 2248–2256.
Peacock, J.D., Lu, Y., Koch, M., Kadler, K.E., Lincoln, J., 2008. Temporal and spatial expression of collagens during murine atrioventricular heart valve development and maintenance. Developmental Dynamics: An Official Publication of the American Association of Anatomists 237, 3051–3058.
Person, A.D., Klewer, S.E., Runyan, R.B., 2005. Cell biology of cardiac cushion development. International Review of Cytology 243, 287–335.
Sato, M., Theret, D.P., Wheeler, L.T., Ohshima, N., Nerem, R.M., 1990. Application of the micropipette technique to the measurement of cultured porcine aortic endothelial cell viscoelastic properties. Journal of Biomechanical Engineering 112, 263–268.
Sedmera, D., Pexieder, T., Rychterova, V., Hu, N., Clark, E.B., 1999. Remodeling of chick embryonic ventricular myoarchitecture under experimentally changed loading conditions. The Anatomical Record 254, 238–252.
Tan, J.L., Tien, J., Pirone, D.M., Gray, D.S., Bhadriraju, K., Chen, C.S., 2003. Cells lying on a bed of microneedles: an approach to isolate mechanical force. Proceedings of the National Academy of Sciences of the United States of America 100, 1484–1489.
Theret, D.P., Levesque, M.J., Sato, M., Nerem, R.M., Wheeler, L.T., 1988. The application of a homogeneous half-space model in the analysis of endothelial cell micropipette measurements. Journal of Biomechanical Engineering 110, 190–199.
Vermot, J., Forouhar, A.S., Liebling, M., Wu, D., Plummer, D., Gharib, M., Fraser, S.E., 2009. Reversing blood flows act through klf2a to ensure normal valvulogenesis in the developing heart. PLoS Biology 7, e1000246.
von Dassow, M., Strother, J.A., Davidson, L.A., 2010. Surprisingly simple mechanical behavior of a complex embryonic tissue. PloS One 5, e15359.
Yalcin, H.C., Shekhar, A., McQuinn, T.C., Butcher, J.T., 2011. Hemodynamic patterning of the avian atrioventricular valve. Developmental Dynamics: An Official Publication of the American Association of Anatomists 240, 23–35.
Zhao, R., Sider, K.L., Simmons, C.A., 2011. Measurement of layer-specific mechanical properties in multilayered biomaterials by micropipette aspiration. Acta Biomaterialia 7, 1220–1227.
Zhao, R., Wyss, K., Simmons, C.A., 2009. Comparison of analytical and inverse finite element approaches to estimate cell viscoelastic properties by micropipette aspiration. Journal of Biomechanics 42, 2768–2773.